Nanoscale

PAPER

View Article Online
View Journal | View Issue

Cite this: *Nanoscale*, 2018, **10**, 5975

Insight into fast ion migration kinetics of a new hybrid single Li-ion conductor based on aluminate complexes for solid-state Li-ion batteries†

Yancong Feng,‡[a,b] Rui Tan,‡[b] Yan Zhao,[b] Rongtan Gao,[b] Luyi Yang,[b] Jinlong Yang,[b] Hao Li,[a] Guofu Zhou,[a] Haibiao Chen[b] and Feng Pan *[b]

Received 21st January 2018,
Accepted 17th February 2018

DOI: 10.1039/c8nr00573g

rsc.li/nanoscale

A novel hybrid single Li-ion conductor (SLIC) for a Li-ion solid electrolyte was prepared by mixing aluminate complexes–polyethylene glycol (LiAl–PEG) and polyethylene oxide (PEO) for solid-state Li-ion batteries. The LiAl–PEG/PEO blend possesses high thermal stability and electrochemical stability with an oxidation decomposition voltage up to 4.8 V. Notably, this hybrid SLIC exhibits not only excellent Li-ion migration kinetics, but also good ionic conductivity as high as 4.0×10^{-5} and 2.6×10^{-4} S cm^{-1} at 30 and 100 °C, respectively, which is much higher than previously reported SLICs. Importantly, by the combination of molecular dynamics simulations and experiment measurements, the mechanisms of Li-ion migration across the SLIC (LiAl–PEG), the salt-in-polymer ($LiClO_4$/PEO) and the optimized SLIC (LiAl–PEG/PEO) were systematically investigated for the first time. The new hopping transport mechanism was verified for the SLIC system at the nanoscale. As for the hybrid SLIC, PEO chains enhance the segmental mobility of the ether-chains bonded with Al atoms, improve the ionicity, and provide extra ionic paths for Li transfer, resulting in the optimized Li-ion migration kinetics of LiAl–PEG/PEO.

1. Introduction

To meet the requirements of advanced solid Li-ion batteries (LIBs), solid polymer electrolytes (SPEs) with superior safety have drawn much attention from researchers.[1–3] Differing from the traditional liquid electrolytes, SPEs have a lot of advantages, such as better processibility and excellent thermal ability.[4,5] Currently, the most typical kind of SPE is the salt-in-polymer, which contains multiple ions migrating between the anode and the cathode.[6,7] This is exactly the main issue of the SPEs, as the migration and accumulation of anions at the interfaces between the electrolytes and the electrodes can result in concentration polarization, further producing "parasitic current" which severely influences the capacity and the cycling life of LIBs. However, it is a very big challenge to address this issue in the SPE systems, owing to the intrinsic characteristics (*e.g.* high viscosity) of SPEs.[8]

In order to restrain the transfer of unnecessary anions and optimize the properties of SPEs, single Li-ion conductors (SLICs) as a new type of solid electrolyte were proposed, which, on the one hand, possess the advantages of SPEs, and on the other hand, have the intrinsic ability to reduce the effects from concentration polarization caused by transferring anions. Nowadays, there are three main types of SLICs, which are organic polymers,[9–11] organic–inorganic hybrid polymers[12–15] and anion acceptors.[16,17] The former two types are the main research focuses in this field. In detail, the space volume and molecular weight of anions could be efficiently improved by forcing the anions to be bonded with polymer chains or restricted in inorganic frameworks, which further restrict the anion movement. Anion-immobilization can prevent concentration polarization, reduce the internal resistance and improve cation migration.[18–20] The features of SLICs based on polymers are that (1) the anions can be anchored in the matrix of the polymer, which does not possess the ability to assist Li-ion migration, and (2) some specific SLICs formed by copolymerization and grafting have structural units (*e.g.*, $-CH_2-CH_2-O-$) that can help Li-ions migrate efficiently. The first reported SLIC was prepared by blending PEO and two other polyanionic addition polymers containing alkyl sulphonic acid and perfluoroalkyl carboxylic acid.[21] At 100 °C, the ionic conductivity

[a]*Guangdong Provincial Key Laboratory of Optical Information Materials and Technology & Institute of Electronic Paper Displays, South China Academy of Advanced Optoelectronics, South China Normal University, Guangzhou 510006, P. R. China*
[b]*School of Advanced Materials, Peking University Shenzhen Graduate School, Shenzhen 518055, P. R. China. E-mail: panfeng@pkusz.edu.cn*
†Electronic supplementary information (ESI) available. See DOI: 10.1039/c8nr00573g
‡These authors contributed equally.

Table 1 Comparison of different single Li-ion conductors based on the anionic structure, type of electrolyte, glass transition temperature (T_g) and Li-ion (σ) conductivity

Anionic structure	Type of electrolyte	T_g/°C	σ_1/S cm^{-1} (RT)	σ_2/S cm^{-1} (high temperature)	Ref.
–$SO_2N(-)SO_2CF_3$	Blend polymer	—	1.1×10^{-10}	1.0×10^{-6} (100 °C)	10
–$SO_2N(-)SO_2CF_3$	Random copolymer	−64	3.0×10^{-6}	$1.0 \times 10^{-4.5}$ (80 °C)	23
–$(C_2O_4)_2B^-$	Random copolymer	−53	1.9×10^{-7}	1.0×10^{-5} (100 °C)	24
–$OP(-)(C_2O_4)_2$	Homopolymer	−47	1.6×10^{-6}	—	25
–$C_6H_5SO_3^-$	Blend polymer	—	3.0×10^{-8}	2.1×10^{-6} (50 °C)	26
–COO^-	Block copolymer	−11	1.0×10^{-7}	1.0×10^{-5} (90 °C)	27
PEO-PS–$SO_2N(-)SO_2CF_3$	Block copolymer	—	1.0×10^{-8}	2.0×10^{-5} (90 °C)	22
PS–$SO_2N(-)SNOCF_3SO_2CF_3$	Block copolymer	44	1.0×10^{-7}	1.4×10^{-4} (90 °C)	9
PEG–Al(−)–PEG–Al(−)	Cross-linked polymer	5.1	3.1×10^{-6}	9.0×10^{-5} (100 °C)	This Work
PEG–Al(−)–PEG–Al(−)/PEO	Blend polymer	—	4.0×10^{-5}	2.6×10^{-4} (100 °C)	This Work

of such an SLIC is up to ~10^{-5} S cm^{-1}. A single-ion triblock polymer (PS–PEO–PS) reported by Armand was used as a solid electrolyte with an ionic conductivity of 1.3×10^{-5} S cm^{-1} operated at 60 °C.[22] The anionic structure, type of electrolyte, glass transition temperature and Li-ion conductivity of recently reported SLICs used in LIBs are summarized in Table 1. Apparently, the ionic conductivity of any listed SLIC is lower than ~10^{-5} S cm^{-1} at room temperature, which seems impractical for applications in LIBs. Therefore, it is important to enhance the Li-ion conductivity, as well as to harness the intrinsic superiority of the SLIC to suppress concentration polarization, and to reveal the related mechanism.

The ionic conductivity of an SLIC is a key property determining whether SLICs can be utilized in LIBs.[28] Nonetheless, there are few reports about the effective ways to optimize the ionic conductivity of SLICs. To obtain SLICs with high performance, we proposed a novel design, in which heterogeneous polyether can be added to assist Li-ion migration and simultaneously improve the Li-ion conducting ability of the anionic framework. As reported,[29] polymers with ether groups do have a promoting impact on Li-ion migration. Herein, an organic–inorganic hybrid SLIC was synthesized from lithium aluminum hydride ($LiAlH_4$) and polyethylene glycol (PEG) using a solvothermal process. The results showed that the ether chains with different lengths diversely contributed to the Li-ion migration. As a consequence, the ionic conductivity of LiAl–PEG (PEG, M_w = 200) was 3.1×10^{-6} and 9.0×10^{-5} S cm^{-1} at 30 and 100 °C, respectively. In order to enhance the electrochemical performance, 15 wt% polyethylene oxide (PEO) was added to supply extra Li-ion transfer paths and to adjust the segmental ability of LiAl–PEG. The ionic conductivity of the conductor was immensely increased by about one order to 4.0×10^{-5} and 2.6×10^{-4} S cm^{-1} at 30 and 100 °C, respectively. More importantly, molecular dynamics simulation was carried out to investigate the mechanisms of the Li-ion migration within the SLIC (LiAl–PEG), the salt-in-polymer ($LiClO_4$/PEO) and the optimized SLIC (LiAl–PEG/PEO), demonstrating that PEO chains optimize the segmental mobility of the ether-chains bonded with Al-ions and provide extra ionic paths for Li-ion transfer. These results are consistent with the enhanced ionic conductivity of LiAl–PEG/PEO. This feasible and novel design can be utilized to optimize and develop new hybrid SLICs in the future.

2. Materials and methods

2.1. Synthesis of LiAl–PEG200

The novel LiAl–PEG200 was synthesized through the condensation polymerization of lithium aluminum hydride ($LiAlH_4$) and polyethylene glycol (PEG, M_w = 200). First of all, 5.0 g of PEG was dissolved in 20 mL of dry tetrahydrofuran (THF) under a nitrogen atmosphere and then the clear solution was stirred at 45 °C for one hour. After this, 12.5 mL of lithium tetrahydridoaluminate tetrahydrofuran solution (containing 6.25 mmol $LiAlH_4$) was added dropwise with a constant pressure dropping funnel. The reaction was held under reflux for 24 h. After the reaction was completed, the THF was removed and the remaining transparent solid jelly was washed with dry THF. Finally, the product was transferred into an Ar-filled glove box and dried at 80 °C for 12 h.

2.2. Preparation of LiAl–PEG/PEO membrane

The obtained LiAl–PEG was dispersed in dry chloroform and the mixture was stirred vigorously at 60 °C for 24 h. Then different contents (5 wt%, 10 wt%, and 15 wt%) of polyethylene oxide (PEO, $M_w = 4 \times 10^6$) and moderate acetonitrile were added into the above dispersion solution. The mixture was stirred for another 24 h to form a homogenous viscous colloid. After this, the obtained mixture was cast onto a Teflon substrate and heated at 80 °C for 12 h to evaporate the solvent and form a transparent membrane. Finally, we obtained the LiAl–PEG/PEO membrane.

2.3. Preparation of the LFP/hybrid electrolytes/Li-ion batteries

The working electrodes were prepared by mixing lithium iron phosphate (LFP), carbon black (CB) and poly(vinylidene fluoride) (PVDF) with a weight ratio of 5 : 3 : 2. Then the electrodes were dried at 80 °C for 24 h in a vacuum oven. The 2032-type coin cells were assembled by stacking up the LFP plate, Al–PEG/PEO membrane, and Li plate seriatim.

2.4. Materials characterization

The morphology of the LiAl–PEG/PEO membrane was observed by field-emission scanning electron microscopy (SEM, ZEISS Supra 55) and elemental mapping was analyzed by energy dispersive spectroscopy. Thermogravimetric analysis was conducted under a nitrogen atmosphere at a heating rate of 5 °C min^{-1} by a TGA/DSC1 system to analyze the thermal stability. The glass transition temperature (T_g) and melt temperature (T_m) were identified by DSC (DSC1). The characteristic spectrum of PEG and LiAl–PEG was studied by FTIR (Frontier). The nuclear magnetic resonance (NMR) spectra (1H NMR) with a chloroform solvent were recorded on a Bruker DPX 400 MHz spectrometer.

2.5. Electrochemical measurements

The electrochemial characterization tests were conducted with a CHI 660E electrochemical workstation. For the EIS and ionic conductivity, the electrolyte membranes were caught sandwiched between two stainless steel block electrodes in coin cells (Fig. S1a†), which were measured from 10 kHz to 0.1 Hz. To test the electrochemical stability of the hybrid membranes, single-ion conductors were sandwiched between the block electrode (stainless steel) and the lithium metal as an integration sealed in coin cells shown in Fig. S1b.† These cells were studied at a scan rate of 0.2 mV s^{-1} between 0 V and 8 V.

Regarding the transfer number of Li-ions, the targeted electrolyte membranes were sandwiched between two lithium metal slices and then sealed in coin cells as seen in Fig. S1c.† Thereafter, by a potentiostatic method, the current changes of the cells were recorded at a constant voltage 10 mV. In addition, the resistance changing situation was detected by EIS tests.

The charge/discharge tests were carried out on a Land instrument (Wuhan Land electronic Co., Ltd, China) with a potential range between 2.0 V (discharge) and 4.2 V (charge). The specific capacities of the batteries are shown in Fig. S2.†

2.6. Model of molecules

The explicit atom model was used to build the molecules in the *Materials Studio* package. In the LiAl–PEG chain, one Al atom links four PEG chains by the Al–O bonds. In the simulation, one LiAl–PEG chain contains 17 Al atoms (shown in Fig. S3†), and each PEG segment consists of 4 repeat units, corresponding to M_w = 200. The Li atoms, distributed randomly in the initial model, have the same molar ratio as that of Al atoms. For the LiAl–PEG system, 10 chains were built. In the LiAl–PEG/PEO blend, 7 LiAl–PEG chains and 6 PEO chains were built. The PEO chain consists of 120 repeat units, and has about half of the mass of LiAl–PEG, *i.e.* there are 15 wt% PEO chains in the system which correspond to the content in the experiment. For comparison with the LiAl–PEG system, the $LiClO_4$/PEO mixture contains 20 PEO chains and 170 $LiClO_4$ groups.

2.7. Details of simulation method

The force field of the CVFF potential from the *Materials Studio* MD code was adopted, and all the simulations were run using the *LAMMPS* package.[30] A multiple time step second-order symplectic integrator (RESPA) was employed with an integration time step of 1 fs for the bond, the angle and torsion forces, 2 fs for the non-bonded van der Waals forces, and 4 fs for the long-range Coulomb interactions, similar to ref. 31. The cut-off distances for the non-bonded interactions were 10 Å. Firstly, the *NPT* ensemble was adopted in the simulations for 10 ns, where the temperature was mostly fixed at T = 453 K, and the pressure was set as P = 0 bar, by using the Nose–Hoover thermostat and barostat. Then the system was cooled to T = 393 K at a rate of 5 K ns^{-1}. The system was relaxed at T = 393 K for above 10 ns and the equilibrium value of the volume was obtained. Secondly, the *NVT* ensemble was adopted at T = 393 K for 50–100 ns with different systems to make sure that the systems reached the equilibrium states, as seen in Fig. S4.† The data of following 350–450 ns were collected for analyses. For observing the migration path of Li-ions, an external electric field was added with an intensity equaling 0.2 V $Å^{-1}$ and with 10–50 ns for different systems to make sure that the displacements of Li-ions in the direction of the electric field are greater than the corresponding length of the box.

3. Results and discussion

The aluminate polymer complex (LiAl–PEG) can be prepared by a facile method. Lithium aluminum hydride ($LiAlH_4$) and polyethylene glycol (PEG) were mixed in the tetrahydrofuran solvent. Thereafter the mixture was stirred at 45 °C for 24 hours. According to the reported analyses,[13,32] three hydrogen atoms of $LiAlH_4$ can react with ether-chains to form a polycondensate network –AlH–$(PEG)_3$–AlH–$(PEG)_3$–, as shown in Fig. 1. Then the intermediate product was heated at 80 °C for 24 h, during which the residual hydrogen atoms can further react with PEG chains. Finally, LiAl–PEG, a new type of SLIC, was obtained.

FTIR, NMR and TGA/DSC were carried out to investigate the basic characteristics of LiAl–PEG and the results are shown in Fig. 2. From the FTIR patterns (Fig. 2a), different from PEG, LiAl–PEG has typical vibration peaks at 1652, 1062, and 691 cm^{-1}. The bending stretch vibrations (691 cm^{-1}) can be labeled as Al–O and the high peak at 1062 cm^{-1} indicates the anti-symmetric vibrations of Al–O–C. ^{1}H NMR was carried out and the characteristic H is marked in the organic structures as shown in Fig. 2b. Differing from PEG, the H marked as 'i' apparently disappeared in the ^{1}H spectrum of LiAl–PEG, indicating that the terminal hydroxyl groups thoroughly reacted with $LiAlH_4$.

The thermal characteristics of LiAl–PEG are presented in Fig. 2c. At 125 °C, LiAl–PEG starts to lose weight due to a certain amount of water absorbed prior to the testing process. According to the DSC curve, LiAl–PEG begins to decompose and releases heat at 350 °C. The TGA/DSC results show that

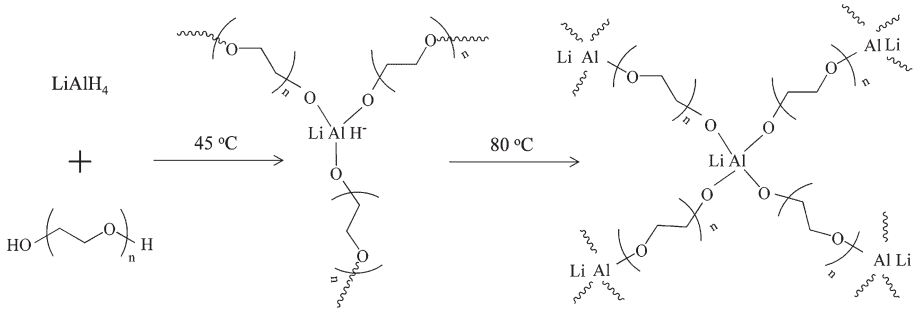

Fig. 1 Chemical reaction for the synthesis of a single Li-ion conductor, LiAl–PEG.

this LiAl–PEG has a superior thermal stability. In order to further study the phase transformation, DSC was carried out from −70 to 100 °C, showing that the T_g of LiAl–PEG is as high as 5.1 °C (inset of Fig. 2c). Since the glass transition temperature (T_g) is the pivotal factor reflecting the levels of segmental mobility, the high T_g proves that ether-chains are anchored by anions to form a whole uniform network with little ability to move. The results of FTIR and TGA/DSC demonstrate that the ether chains are cross-linked by Al-ions as centers and the segmental mobility of the ether chains are restrained by a cross-linked structure, creating a typical circumstance in which only Li-ions can migrate.

For analyzing the electrochemical features of LiAl–PEG with different molecular weights, LiAl–PEG200, LiAl–PEG400, and LiAl–PEG600 materials were prepared as the electrolyte membranes. Fig. 3a shows the impedance of LiAl–PEG200/PEO at different temperatures measured by electrochemical impedance spectroscopy (EIS). At room temperature, the value of impedance is 4228 Ω. With the temperature increasing, the contact between the electrolyte and the block electrodes is promoted. At 80 °C, the value of the impedance is only 51 Ω. Without the addition of PEO, the impedance value of LiAl–PEG200 (inset of Fig. 3a) is as high as 31.7 kΩ, indicating that PEO chains optimize the segmental mobility and further accelerate Li migration.

Transfer number is a key factor for the single-ion conductor, which can be obtained according to eqn (1):

$$t_+ = \frac{I_{ss}(\Delta V - I_0 \times R_0)}{I_0(\Delta V - I_{ss} \times R_{ss})} \quad (1)$$

where I_o and I_{ss} are the initial current and the final current at a constant voltage with ΔV, respectively. R_o and R_{ss} are the initial and final resistances. After 5000 seconds, the value of the current becomes stable and all the related parameter values are shown in Fig. 3b. According to eqn (1), the calculated transfer number of the Li-ion is 0.98, confirming that only Li-ions can migrate into this hybrid corresponding to our design thought. Apart from the transfer number, the electrochemical stability of the electrolyte, which directly determines the available application range of cathode and anode materials, is also very crucial. The electrochemical stabilities of LiAl–PEG200, LiAl–PEG400, LiAl–PEG600 and LiAl–PEG200/PEO were studied by the cyclic voltammetry (C–V) method. From Fig. 3c, the oxidation potential of LiAl–PEG200/PEO is about 4.8 V, higher than those of LiAl–PEG200, LiAl–PEG400 and LiAl–PEG600 (4.0, 3.7 and 3.8 V). In order to confirm the veracity, the curve of LiAl–PEG200/PEO was enlarged as seen in the inset of Fig. 3c. At ~3.5 V, the oxidation reaction had already occured. However, with the addition of PEO, the extent of this vice reaction is weak as the reaction current is very low. After the experimental tests of Li-ion kinetics, conductivities and electrochemical stabilities, the electrochemical performances of batteries were tested. From Fig. S2,† the reversible capacity of $LiFePO_4$ (LFP) as the cathode and Li metal as the anode batteries is 162.9 mA h g^{-1} at 0.5 C, indicating that Li-ions can successfully move between the electrodes.

The EIS data of LiAl–PEG200, LiAl–PEG400, LiAl–PEG600, LiAl–PEG200/PEO and $LiClO_4$/PEO were also utilized to investigate the Li-ion kinetic properties. The ionic conductivity can be obtained using eqn (2):[33,34]

$$\sigma = L/(R_{ohm} \times S) \quad (2)$$

where L is the thickness of the membrane film, R_{ohm} is the impedance tested by EIS and S is the area of the electrolyte membrane. Among the LiAl–PEG electrolytes, LiAl–PEG200 with high Li-ion concentration has the highest ionic conductivity (3.1×10^{-6} and 9.0×10^{-6} S cm^{-1} at 30 and 100 °C, respectively). Notably, the added PEO can effectively promote the Li-ion kinetic properties. The ionic conductivity of LiAl–PEG200 is immensely improved, as high as 4.0×10^{-5} and 2.6×10^{-4} at 30 and 100 °C, respectively. Herein, by fitting the ionic conductivity data of LiAl–PEG200, LiAl–PEG400, LiAl–PEG600, and LiAl–PEG200/PEO, it is clear that the logarithms of the ionic conductivity show an approximately linear relation with $1/T$ from 30 to 100 °C as seen in Fig. 4a. A typical model is needed to explain these consecutive curves, in which the linear part corresponds to the Arrhenius eqn (3):[5]

$$\sigma = A \exp\left(-\frac{E_a}{RT}\right) \quad (3)$$

where A is the pre-exponential factor and E_a is the activation energy for conductivity. The Arrhenius behavior is generally known as a typical type, in which Li-ions can hop through the sites in the electrolyte and decouple from the long-range mobi-

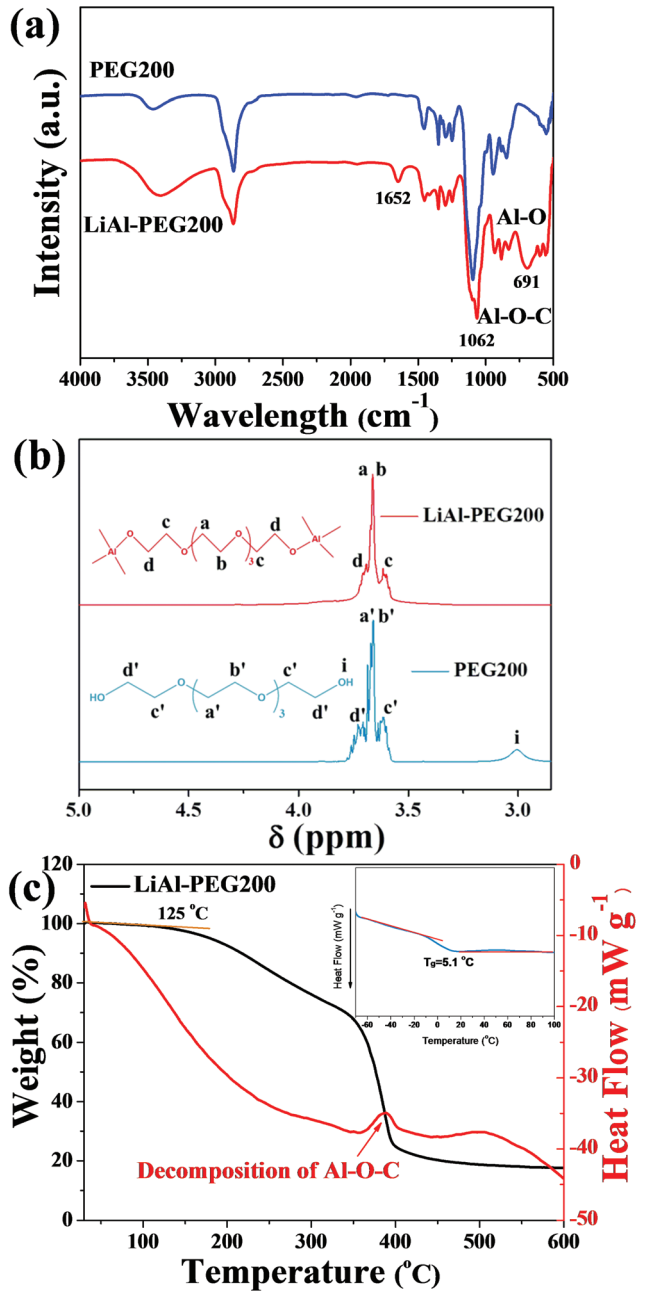

Fig. 2 (a) FTIR spectra of LiAl–PEG and PEG from 4000 to 400 cm^{-1}, (b) ^1H NMR of LiAl–PEG and PEG, and (c) DSC/TGA curves of LiAl–PEG (inset is the DSC curve of LiAl–PEG for −70 to 100 °C). LiAl–PEG200 in this figure is the same as LiAl–PEG in the text.

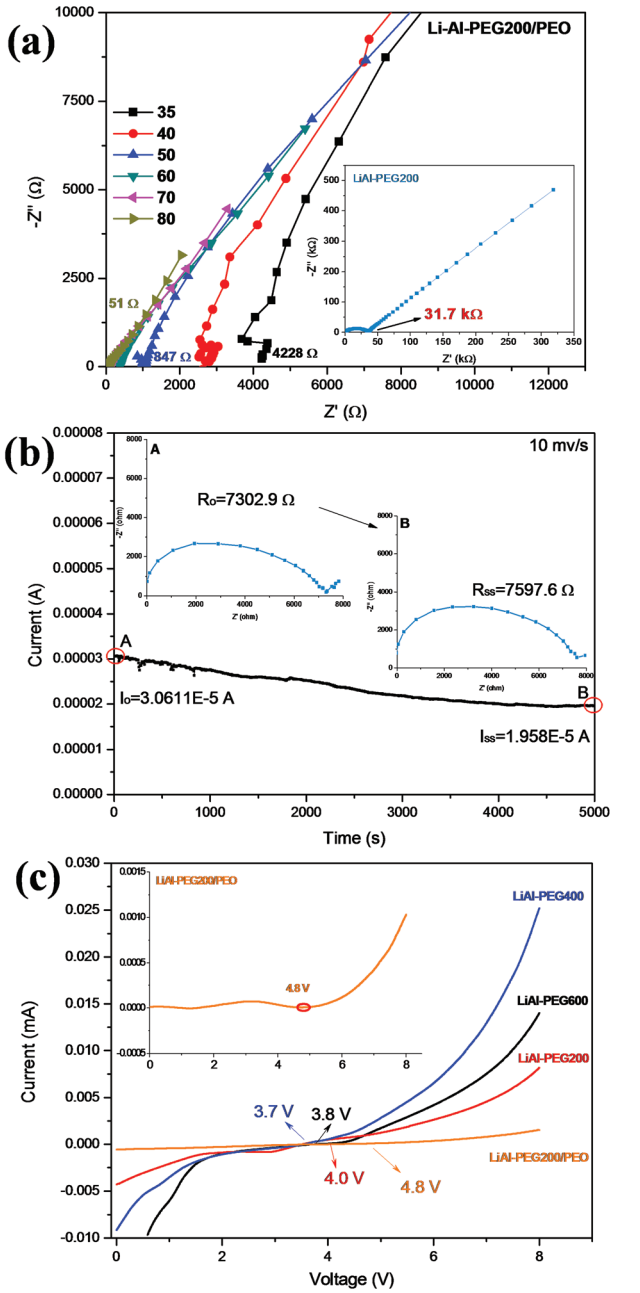

Fig. 3 (a) EIS plots of LiAl–PEG200/PEO at different temperatures, (b) transfer number measurement results of LiAl–PEG/PEO and (c) electrochemical stabilities of LiAl–PEG200, LiAl–PEG400, LiAl–PEG600 and LiAl–PEG200/PEO.

lity of the matrix.[5] The result further proves that the Li-ion transport undergoes a hopping cycle, in which a Li-ion dissociates from the anchored anion, then hops through the ether units, and thereafter recombines with another anion. The length of the ether chain connecting two adjacent anchored anions can influence Li-ion transfer mobility. For example, LiAl–PEG600 has a longer migration distance than that of LiAl–PEG200, explaining the reason why LiAl–PEG200 has a much higher ion conductivity. On the other hand, the ion conductivity of LiAl–PEG200/PEO is obviously higher than that of LiAl–PEG200. PEO chains may work as an additive to optimize the segmental mobility of the ether-chain bonded with Al-ions and also provide extra ionic paths for Li transfer.

The classical salt-in-polymer system ($LiClO_4$/PEO system) is adopted for comparison with the new SLIC. From Fig. 4b, the Li-ion transferring model in the $LiClO_4$/PEO system can be classified as VTF behavior, indicating Li-ion migration coup-

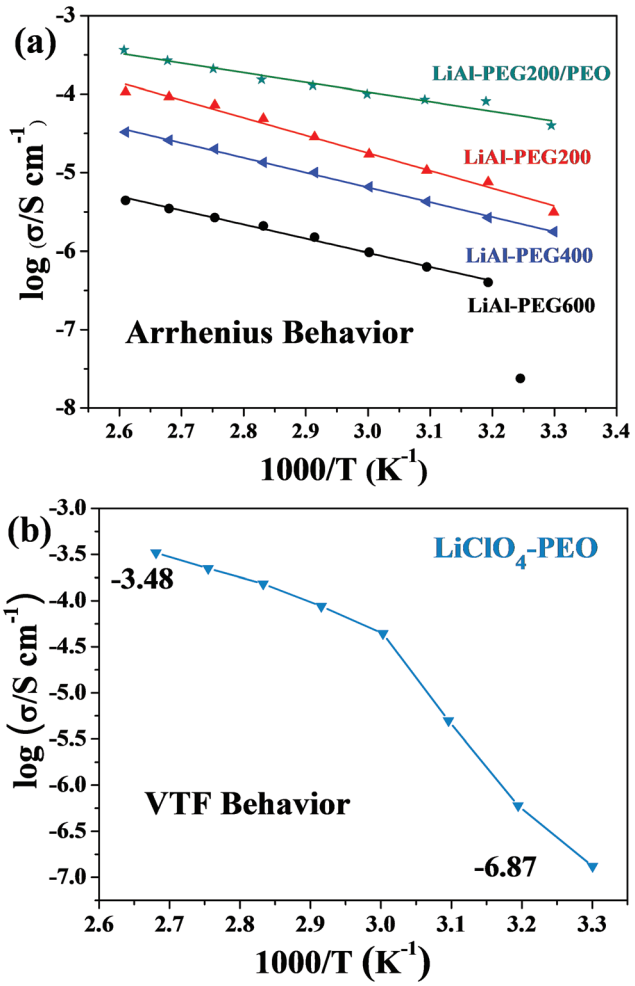

Fig. 4 (a) Arrhenius plots of the ionic conductivity with varied temperatures and the fitting curves for LiAl–PEG200, LiAl–PEG400, LiAl–PEG600 and LiAl–PEG200/PEO. (b) VTF behavior of the $LiClO_4$/PEO system.

ling with the polymer branches.[5] The VTF behavior is more relevant for the polymer electrolyte and is described by eqn (4):

$$\sigma = \sigma_0 T^{-\frac{1}{2}} \exp\left(-\frac{B}{T - T_0}\right) \quad (4)$$

where B is the pseudo-activation energy for the conductivity, and T_0 is the reference temperature which normally falls 10–50 K below the experimental glass transition, T_g. This behavior is related to the ion motion coupled with the long-range motions of polymer branches or solvent molecules, corresponding to classical polymer electrolytes, $LiClO_4$/PEO. These two electrical behaviors prove that the Li-ion migration into LiAl–PEG is different from that in PEO containing lithium salts.

Investigating the mechanism of Li-ion migration across the SLIC (LiAl–PEG), salt-in-polymer ($LiClO_4$/PEO) and optimized SLIC (LiAl–PEG/PEO) is the key emphasis in our work. According to previous research studies,[35–38] since the anions are anchored on the polymer chains in the SLIC systems, the Li-ions can hop through the sites involved in the conducting network. As for the salt-in-polymer, the movement of Li-ions couples with the long-range motion of the polymer chains, such as ether chains. The polymer chains can act as a very good solvent for the Li-ions. Moreover, according to the experimental results, the SLIC/PEO blend possesses superior Li-ion kinetic behavior, in which the additive PEO plays a vital role. However, no previous research has investigated the function of polymer chains (ether) added in the SLIC system and the mechanism of the optimized SLIC system. Therefore the ionic conductivity, conformational dynamics of the polymer chain and ionicity of the three systems (LiAl–PEG, $LiClO_4$/PEO, and LiAl–PEG/PEO) were studied by the molecular dynamics simulation method.

Firstly, the ionic conductivities of the three systems were calculated. The ionic conductivity (κ) was extracted using the Einstein relation (5):

$$\kappa = \lim_{t\to\infty} \frac{e^2}{6tVk_BT} \sum_{i,j}^{N} Z_i Z_j \langle (R_i(t) - R_i(0))(R_j(t) - R_j(0)) \rangle \quad (5)$$

where e is the electron charge, V is the volume of the simulation box, k_B is the Boltzmann constant, T is the temperature, t is the time, z_i and z_j are the Li-ionic and anionic charges, and $R_i(t)$ is the displacement of the ion i during the time t. At 393 K, the ionic conductivities of the LiAl–PEG, LiAl–PEG/PEO and $LiClO_4$/PEO systems are 3.2×10^{-6}, 9.1×10^{-6} and 7.3×10^{-5}, respectively. The qualitative comparisons of the ionic conductivities are the same by calculation and experiment methods. The self-diffusion coefficients (D) of the Li-ion and anion are shown in Fig. S6.† The qualitative comparison of the self-diffusion coefficients is the same as that of the calculated ionic conductivity.

Moreover, it is known that in the salt-in-PEO, the Li cation is solvated in the PEO host in a way that the PEO segment wraps around the cation; in the LiAl–PEG, the Li cation can hop through the anchored ether-chains. As a consequence, the Li-ion transmission is related to the conformational dynamics of the ether-chain. Fig. 5a and b show the probabilities of the torsional angles for the –O–C–C–O– and –C–C–O–C– dihedrals, respectively. The peak-valleys emerge at −120°, 0° and 120°, as well as the definition in ref. 39, the *trans*, *gauche*$^+$ and *gauche*$^-$ dihedral states are ranged in $|\phi| \geq 120°$, $-120° < \phi < 0°$ and $0° < \phi < 120°$, respectively. Fig. 5c shows the schematic of the conformational transition. The average conformational transition rate is defined as the average number of transitions per dihedral divided by the total trajectory time. Table 2 presents the conformational transition rates (ns^{-1}) of the LiAl–PEG, LiAl–PEG/PEO and $LiClO_4$/PEO mixtures. The conformational transition rate of the PEG segment in LiAl–PEG/PEO is higher than that in LiAl–PEG, indicating that the addition of PEO can enhance the polymer chain mobility. Comparing the LiAl–PEG/PEO with the $LiClO_4$/PEO, the conformational transition rate of PEO in the former is higher. The reason accounted for the low conformational transition ability of the $LiClO_4$/PEO

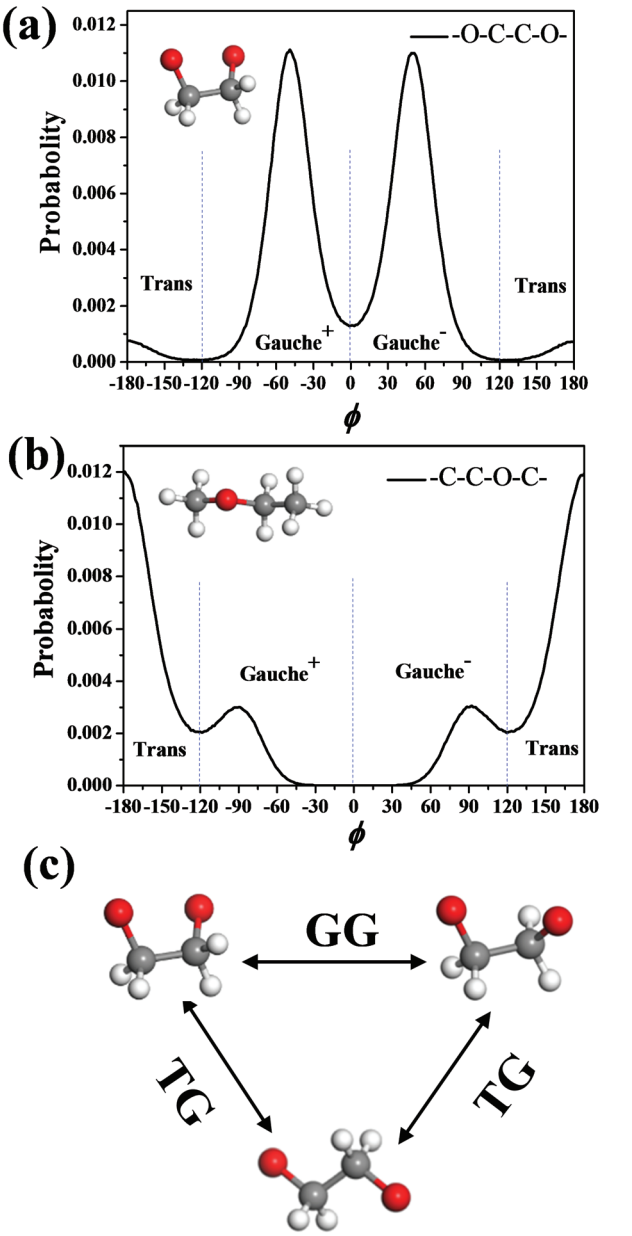

Fig. 5 Probabilities of the torsional angles for (a) –O–C–C–O– and (b) –C–C–O–C– dihedrals. (c) Schematic of the conformational transition among the *trans* (T), *gauche*$^+$ (G^+) and *gauche*$^-$ (G^-) dihedral states of the –O–C–C–O– dihedral.

system is that all the ions are solved in the PEO chains, restricting the conformational transition rate. Similarly, as to the LiAl–PEG, most of the ions that existed in the LiAl–PEG domain can have an influence on the conformational transition ability of the anchored ether chains. Thus, the added PEO is able to optimize the conformational transition ability of the ether-chains involved in the LiAl–PEG, further promoting the kinetics of Li-ions.

The Li-ion transport mechanisms of the three systems are explored. The distribution of Li-ion displacement can be quantified by computing the time-dependent self-part of the van Hove correlation function $G_s(r, t)$ as:[40]

Table 2 Conformational transition rates (ns^{-1}) of the dihedrals. The LiAl–PEG200 is selected as the SLIC in the simulations, which is named "LiAl–PEG" for simplicity

System	Dihedral	GG	TG	All
LiAl–PEG	–O–C–C–O–	3.648	0.774	4.422
	–C–C–O–C–	0.381	3.217	3.598
LiAl–PEG/PEO				
PEG	–O–C–C–O–	3.841	0.697	4.538
	–C–C–O–C–	0.263	3.343	3.606
PEO	–O–C–C–O–	3.967	1.717	5.684
	–C–C–O–C–	0.466	4.253	4.719
$LiClO_4$/PEO	–O–C–C–O–	4.297	0.748	5.045
	–C–C–O–C–	0.256	3.586	3.842

$$G_s(r,t) = \frac{1}{N}\sum_{i=1}^{N}\langle\delta(r - |\vec{r}_i(t) - \vec{r}_i(0)|)\rangle. \quad (6)$$

The $4\pi r^2 G_s(r, t)$ is the probability that a Li-ion has moved a distance r within the time t. The volume integral of $G_s(r, t)$ is a conserved quantity for all times t, that is

$$\int_0^\infty 4\pi r^2 G_s(r,t)\mathrm{d}r = 1. \quad (7)$$

At a short time t = 1 ns, the functions $4\pi r^2 G_s(r, t)$ of the three systems show a similar tendency and decay rapidly to zero at very short distances, as depicted in Fig. 6a. The function of the LiAl–PEG systems decays at the shortest distance, which corresponds to the lowest self-diffusion coefficient as shown in Fig. S6.† At a large distance and a long time t = 300 ns, the appearance of a secondary peak in the $4\pi r^2 G_s(r, t)$ curve of the LiAl–PEG system proves that the Li-ion hopping process occurs throughout the simulation,[41,42] as shown in Fig. 6b. For the LiAl–PEG/PEO system, an unobvious peak of the curve emerges at about r = 22 Å, indicating that the PEO chains change the pattern of Li-ion migration. The curve of the $LiClO_4$/PEO system is relatively smooth, indicating the continuous process of Li-ion transport.[43]

For further revealing the Li-ion transport mechanism, we compare the single Li-ion conductor (LiAl–PEG) with the salt-in-polymer ($LiClO_4$/PEO). Fig. 7 presents the schematics of the Li-ion transport mechanism under an electric field for the two systems. To the simulated systems was added an electric field in the Z-direction with the electric field intensity equal to 0.2 V $Å^{-1}$. The displacements of ions at different directions under the electric field are shown in Fig. S7.† For the LiAl–PEG system, the Li cations are attracted to the anions, proved by the very high first peak of the Li-anion, as shown in Fig. 7a. Under an electric field, the Li cations decouple from the anions. Although the Al-region occupies 14.8 vol% of the system, the 94.8% of the total Li atoms emerge in this region under an electric field, indicating that the Li cations hop among the anions to transport. For further demonstration of

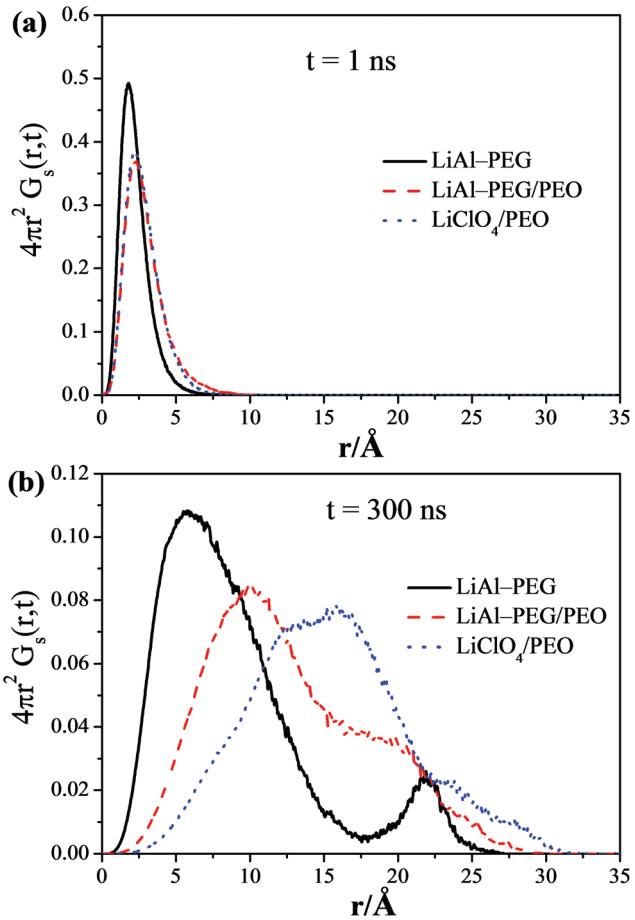

Fig. 6 Self-part of the van Hove correlation functions $4\pi r^2 G_s(r, t)$ of Li-ions at (a) short time t = 1 ns and (b) long time t = 300 ns in the LiAl–PEG, LiAl–PEG/PEO and $LiClO_4$/PEO systems, respectively.

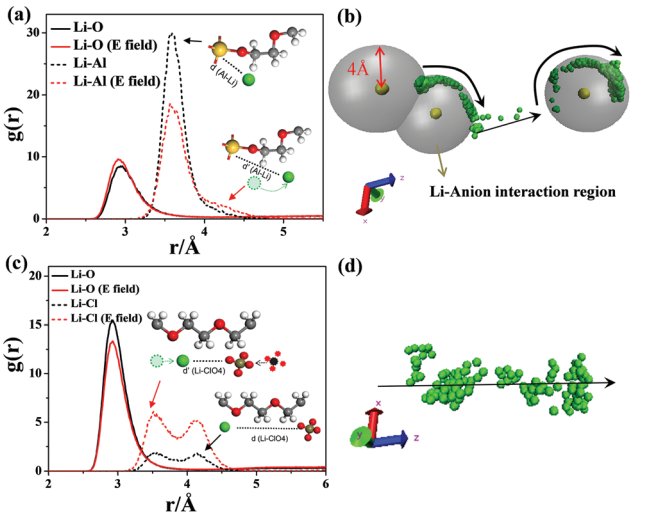

Fig. 7 Schematics of the Li-ion transport mechanism under an electric field for the two systems, supported by the results of the simulations. (a and c) Radial distribution functions and (b and d) snapshots of the Li migration path of the LiAl–PEG and $LiClO_4$/PEO systems, respectively. Note that the O atom calculated in (a) and (c) is in the ether chain, excepting for the one bonded with the Al atom. The trajectory was recorded every 5 ps. For clarity, the trajectories of Li are displayed every 5 ps and 25 ps in LiAl–PEG and $LiClO_4$/PEO, respectively.

the hopping transport mechanism, the discontinuous trajectory of one Li atom is shown in Fig. 7b.

In Fig. 7c, corresponding to the $LiClO_4$/PEO mixture, the low peak of the Li–anion and the high peak of Li–O indicate that the Li cations are surrounded by PEO chains without an electric field. The peaks of the Li–anion increase whereas the one of Li–O drops after applying the electric field, which is opposite to the phenomenon of the LiAl–PEG system. The decoupling between Li-ions and oxygen atoms occurs and the coupling between Li^+ and ClO_4^- gradually enhances. The continuous trajectory of one Li atom and the schematic of the model are presented in Fig. 7d, indicating the different transport mechanisms compared with that of the pure LiAl–PEG system.

Comparing Fig. 7b and d, it can be seen that the Li-ion moves around the anion cluster slowly and hops to another anion quickly in the LiAl–PEG system, whereas the Li-ion transports more "linearly" in the $LiClO_4$/PEO mixture. The ratios of path length to displacement are 50.6 and 19.2 for the LiAl–PEG and $LiClO_4$/PEO systems, respectively. This indicates that the Li atom has a longer path length in the LiAl–PEG system, which is an important reason that the SLIC has a lower conductivity than the salt-in-polymer. On the other hand, we speculate that designing the SLIC with a small action radius of the anion cluster can shorten the transport path length of the Li-ion, improving the ionic conductivity.

Although single Li-ion conductors can reduce the effects from concentration polarization, the low ionic conductivity still limits their application in solid-state Li-ion batteries. The addition of PEO can improve the ionic conductivity of the material, according to the experimental and calculated data. As a good solvent, PEO chains play an important role in dissociating the ion pair. The degree of ion uncorrelated motion (α_d) that is sometimes called ionicity is given by eqn (8) and (9):

$$\alpha_d = \frac{\kappa}{\kappa_{uncorr}} \quad (8)$$

$$\kappa_{uncorr} = \frac{e^2}{VK_BT}(n_+D_+ + n_-D_-) \quad (9)$$

where n_+ and n_- are the number of cations and anions, respectively. The κ_{uncorr} is the ideal conductivity that can be realized if the ion motion is uncorrelated. For the $LiClO_4$/PEO mixture, the relatively high ionicity equal to 0.57 means that all the anions are free to move, potentially causing detrimental effects of anion polarization. The value of α_d is far below 1, indicating that the anion and Li-ion motion is not essentially uncorrelated. On the other hand, low ionicity means the strong interaction between ions and anions, resulting in the high migration barrier of Li-ions, such as in the LiAl–PEG system (α_d = 0.18). PEO acts as a good solvent for the Li-ion, improving the ionicity (α_d = 0.37 in the LiAl–PEG/PEO blend).

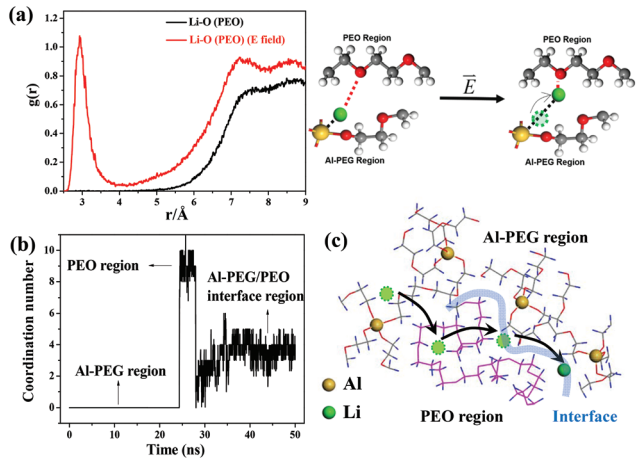

Fig. 8 (a) Radial distribution functions, (b) coordination number of the oxygen atoms on the PEO chains around a selected Li cation, and (c) schematic for the Li-ion transport in the LiAl–PEG/PEO blend.

The role of PEO in the LiAl–PEG complex is further confirmed by the Li 1s XPS spectrum, presented in Fig. S8.†

For the LiAl–PEG/PEO blend, the Li cations are initially coupled to the anions, *i.e.* are in the Al–PEG domain. Under an electric field, the Li cations can migrate from the Al–PEG domain to the PEO domain, or transport along the Al–PEG/PEO interface region, proved by the radial distribution functions as shown in Fig. 8a and described in Fig. 8b. The migration paths can be confirmed by the coordination number of oxygen atoms on the PEO chains around a selected Li cation as presented in Fig. 8b, where the coordination number equaling 0 means that the Li cation is in the Al–PEG domain. In Fig. 7c, corresponding to the $LiClO_4$/PEO mixture, the Li–O coordination number is about 9 with the cut-off distance equaling to r = 4 Å where the first peak of the red solid ends. Therefore, in Fig. 8b, the coordination number equaling about 9, which is close to the value of the $LiClO_4$/PEO system, indicates the existence of Li cations in the PEO domain. In order to find the main migration path, we calculate the ratios of Li cations in the three domains. Almost all the Li cations initially exist in the Al–PEG domain. Under an electric field, 7.7% of the Li cations emerge in the interface region and 0.2% of them move to the PEO domain. Comparing the calculated conductivities between the LiAl–PEG and LiAl–PEG/PEO systems, we speculate that enlarging the interface region can increase conductivity. It guides the investigation experiment that the improvement of the compatibility between the single Li-ion conductor and PEO can increase the conductivity of the batteries.

4. Conclusion

In summary, a hybrid SLIC (LiAl–PEG/PEO) with high Li-ion kinetic ability (4.0×10^{-5} and 2.6×10^{-4} S cm^{-1} at 30 and 100 °C, respectively) was prepared and characterized. In addition, the LiAl–PEG/PEO possesses high thermal stability and electrochemical stability (oxidation decomposition voltage is as high as 4.8 V).

Importantly, the molecular dynamics simulation method was carried out to investigate the mechanism of the Li-ion migration within $LiClO_4$/PEO, LiAl–PEG and LiAl–PEG/PEO based on four key aspects, including the ionic conductivity, conformational dynamics of the polymer chain, diffusion and ionicity. The simulation results show that Li-ions are restrained by the anion cluster, accounting for the low ionic conductivity of LiAl–PEG. The self-part of the van Hove correlation function proves the hopping process of Li-ions. Moreover, a new hopping transport mechanism is proposed, *i.e.*, the Li-ion moves around the anion cluster slowly and hops to another anion cluster quickly in the LiAl–PEG region. Therefore, designing the anion cluster with a small action radius may improve the migration rate of Li-ions.

After adding the PEO additive, PEO chains optimize the segmental mobility of the ether-chain bonded with Al atoms, improve the ionicity, and provide extra ionic pathways for Li-ion transfer, resulting in the optimized conductivity of LiAl–PEG/PEO. Thus, according to the experimental and calculation results, adding a heterogeneous polymer as extra path suppliers and optimizers to enhance the conformational transition ability is a promising approach to promote the electrochemical performances of SLICs.

Conflicts of interest

There are no conflicts of interest to declare.

Acknowledgements

The research was financially supported by the Joint International Research Laboratory of Optical Information, the National Science Foundation of China (No. 51703070, 51602009, 51561135014), the Chinese Postdoctoral Science Foundation (No. 2016M600008, 2017M612686), Shenzhen Science and Technology Research Grant (No. JCYJ20150629144453251), Guangdong Innovation Team Project (No. 2013N080), Shenzhen Science and Technology Research Grant (peacock plan KYPT20141016105435850), and National Materials Genome Project (2016YFB0700600). Thanks to the National Center for the International Research on Green Optoelectronics and MOE International Laboratory for Optical Information Technologies. The support from CHEMCLOUDCOMPUTING of Beijing University of Chemical Technology is greatly appreciated.

References

1 J. B. Goodenough and K. S. Park, *J. Am. Chem. Soc.*, 2013, **135**, 1167–1176.

2 M. Kammoun, S. Berg and H. Ardebili, *Nanoscale*, 2015, **7**, 17516–17522.
3 R. Bouchet, S. Maria, R. Meziane, A. Aboulaich, L. Lienafa, J. P. Bonnet, T. N. Phan, D. Bertin, D. Gigmes and D. Devaux, *Nat. Mater.*, 2013, **12**, 452–457.
4 K. Xu, *Chem. Rev.*, 2004, **104**, 4303–4417.
5 E. Quartarone and P. Mustarelli, *Chem. Soc. Rev.*, 2011, **40**, 2525–2540.
6 L. Y. Yang, D. X. Wei, M. Xu, Y. F. Yao and Q. Chen, *Angew. Chem., Int. Ed.*, 2014, **53**, 3631–3635.
7 J. F. M. Oudenhoven, L. Baggetto and P. H. L. Notten, *Adv. Energy Mater.*, 2011, **1**, 10–33.
8 K. Xu, *Chem. Rev.*, 2014, **114**, 11503–11618.
9 Q. Ma, H. Zhang, C. Zhou, L. Zheng, P. Cheng, J. Nie, W. Feng, Y. S. Hu, H. Li, X. Huang, L. Chen, M. Armand and Z. Zhou, *Angew. Chem., Int. Ed.*, 2016, **55**, 2521–2525.
10 S. Feng, D. Shi, F. Liu, L. Zheng, J. Nie, W. Feng, X. Huang, M. Armand and Z. Zhou, *Electrochim. Acta*, 2013, **93**, 254–263.
11 S. Amaresh, K. Karthikeyan, K. J. Kim, Y. G. Lee and Y. S. Lee, *Nanoscale*, 2014, **6**, 6661–6667.
12 N. Lago, O. Garcia-Calvo, J. M. Lopez del Amo, T. Rojo and M. Armand, *ChemSusChem*, 2015, **8**, 3039–3043.
13 K. Onishi, M. Matsumoto, A. Yoshifumi Nakacho and K. Shigehara, *Chem. Mater.*, 1996, **8**, 469–472.
14 B. K. Mandal, C. J. Walsh, T. Sooksimuang, S. J. Behroozi, S. Kim, Y. Kim, E. S. Smotkin, R. Filler and C. Castro, *Chem. Mater.*, 2000, **12**, 6–8.
15 J. Cao, Y. Shang, L. Wang, X. He, L. Deng and H. Chen, *RSC Adv.*, 2015, **5**, 8258–8262.
16 A. Hekselman, M. Kalita, A. Plewa-Marczewska, G. Z. Żukowska, E. Sasim, W. Wieczorek and M. Siekierski, *Electrochim. Acta*, 2010, **55**, 1298–1307.
17 A. M. Stephan, T. Prem Kumar, N. Angulakshmi, P. S. Salini, R. Sabarinathan, A. Srinivasan and S. Thomas, *J. Appl. Polym. Sci.*, 2011, **120**, 2215–2221.
18 Y. Tang, Y. Zhang, J. Deng, D. Qi, W. R. Leow, J. Wei, S. Yin, Z. Dong, R. Yazami, Z. Chen and X. Chen, *Angew. Chem., Int. Ed.*, 2014, **53**, 13488–13492.
19 Y. Tang, Y. Zhang, W. Li, B. Ma and X. Chen, *Chem. Soc. Rev.*, 2015, **44**, 5926–5940.
20 Y. Zhang, O. I. Malyi, Y. Tang, J. Wei, Z. Zhu, H. Xia, W. Li, J. Guo, X. Zhou, Z. Chen, C. Persson and X. Chen, *Angew. Chem., Int. Ed.*, 2017, **56**, 14847–14852.
21 D. J. Bannister, G. R. Davies, I. M. Ward and J. E. Mcintyre, *Polymer*, 1984, **25**, 1291–1296.
22 R. Bouchet, S. Maria, R. Meziane, A. Aboulaich, L. Lienafa, J. Bonnet, T. N. T. Phan, D. Bertin, D. Gigmes, D. Devaux, R. Denoyel and M. Armand, *Nat. Mater.*, 2013, **12**, 452–457.
23 H. Allcock, D. Welna and A. Maher, *Solid State Ionics*, 2006, **177**, 741–747.
24 X. G. Sun, C. L. R. And and J. B. Kerr, *Macromolecules*, 2004, **37**, 2219–2227.
25 X. G. Sun and C. A. Angell, *Solid State Ionics*, 2004, **175**, 257–260.
26 J. W. Rhim, H. B. Park, C. S. Lee, J. H. Jun, D. S. Kim and Y. M. Lee, *J. Membr. Sci.*, 2004, **238**, 143–151.
27 S. W. Ryu, P. E. Trapa, S. C. Olugebefola, J. A. Gonzalez-Leon, D. R. Sadoway and A. M. Mayes, *J. Electrochem. Soc.*, 2005, **152**, A158–A163.
28 J. F. Van Humbeck, M. L. Aubrey, A. Alsbaiee, R. Ameloot, G. W. Coates, W. R. Dichtel and J. R. Long, *Chem. Sci.*, 2015, **6**, 5499–5505.
29 Y. Tang, J. Deng, W. Li, O. I. Malyi, Y. Zhang, X. Zhou, S. Pan, J. Wei, Y. Cai, Z. Chen and X. Chen, *Adv. Mater.*, 2017, **29**, 1701828.
30 S. J. Plimpton, *J. Comp. Physiol.*, 1995, **117**, 1–19.
31 C. Chen, P. Depa, V. G. Sakai, J. K. Maranas, J. W. Lynn, I. Peral and J. R. D. Copley, *J. Chem. Phys.*, 2006, **124**, 234901.
32 F. Kaneko, S. Wada, M. Nakayama, M. Wakihara, J. Koki and S. Kuroki, *Adv. Funct. Mater.*, 2009, **19**, 918–925.
33 R. Tan, J. Yang, J. Zheng, K. Wang, L. Lin, S. Ji, J. Liu and F. Pan, *Nano Energy*, 2015, **16**, 112–121.
34 D. Zhou, Y.-B. He, R. Liu, M. Liu, H. Du, B. Li, Q. Cai, Q.-H. Yang and F. Kang, *Adv. Energy Mater.*, 2015, **5**, 1500353.
35 S. Dou, S. Zhang, R. J. Klein, A. James Runt and R. H. Colby, *Chem. Mater.*, 2006, **18**, 4288–4295.
36 P. K. Singh, K.-W. Kim and H.-W. Rhee, *Electrochem. Commun.*, 2008, **10**, 1769–1772.
37 A. M. Christie, S. J. Lilley, E. Staunton, Y. G. Andreev and P. G. Bruce, *Nature*, 2005, **433**, 50–53.
38 N. Boaretto, C. Joost, H. Lorrmann, K. Vezzù, G. Pace and V. Di Noto, *J. Phys. Chem. C*, 2016, **120**, 10770–10780.
39 M. Canales, *Phys. Rev. E*, 2009, **79**, 051802.
40 L. V. Hove, *Phys. Rev.*, 1954, **95**, 249–262.
41 M. C. C. Ribeiro, *Phys. Chem. Chem. Phys.*, 2004, **6**, 771–774.
42 Z. Hu and C. J. Margulis, *Proc. Natl. Acad. Sci. U. S. A.*, 2006, **103**, 831–836.
43 Y. L. Wang, B. Li, S. Sarman and A. Laaksonen, *J. Chem. Phys.*, 2017, **147**, 224502.

